ELSEVIER

Journal of Nuclear Materials 258–263 (1998) 694–699

journal of nuclear materials

Section 5.2. Low Z (C, Be, etc.)

Gas bubbles in beryllium implanted with He ions at temperatures $\leqslant 700$ K and after post-implantation annealing

V.N. Chernikov [a], H. Ullmaier [b,*], A.P. Zakharov [a]

[a] *Institute of Physical Chemistry of the Russian Academy of Sciences, Leninsky pr. 31, Moscow 117915, Russian Federation*
[b] *Institut für Festkörperforschung des Forschungszentrum Jülich, GmbH, Postfach 1913, D-52425 Jülich, Germany*

Abstract

Helium bubbles in beryllium implanted with 5 and 15 keV He ions at temperatures, T_{irr}, from 300 to 700 K before and after post-implantation annealing at temperatures, T_{ann}, up to 1100 K have been studied by TEM. Tiny overpressurized He bubbles are observed for $T_{irr} \leqslant 500$ K. At $T_{irr} = 700$ K the bubbles are larger and mainly facetted. At higher fluences coarser and flattened-out gas cavities and labyrinth systems are developed. A qualitative explanation of He reemission data at different irradiation temperatures based on these observations is suggested. An estimate of the dissociation temperature of HeV complexes in Be gives a value of 900 K. The development of the gas porosity during annealing of Be implanted with He ions at $T_{irr} \leqslant 500$ K demonstrates features similar to those of fcc-Ni and Cu, in which a part of He bubbles maintain their overpressure up to 70% of the melting point. Ion irradiation leads to an enhanced growth of a microcrystalline surface layer of cph-BeO which is suspected to act as a barrier for the permeation of thermal vacancies. Finally, the appearance and the parameters of helium bubbles are compared with those of deuterium filled cavities developed under equivalent conditions and the differences are discussed.

1. Introduction

An understanding of the behavior of hydrogen and helium isotopes in beryllium is of great importance for its application in fusion devices [1–4]. These gases are introduced into near-surface regions by implantation from the plasma and into the bulk by neutron-induced nuclear reactions (about $6–7 \times 10^{-4}$ He at.fr./dpa) and tritium decay. Helium is the main reason for Be swelling during neutron irradiation. Indeed, while the upper limit of the vacancy swelling in metals is about $0.5T_m$ (T_m is the melting point), a remarkable swelling of Be is not registered below an irradiation temperature, T_{irr}, of $\approx 0.5T_m \cong 780$ K.

Radiation effects in Be as a fusion material are reviewed by Gelles et al. [5] starting from the pioneer works of Ells et al. [6] and Rich et al. [7]. The degree of radiation swelling and properties of Be strongly depend on its microstructure and testing scenario. In particular, swelling of Be single-crystals under fast neutron irradiation is significantly lower than that of polycrystals (cf. data in Refs. [8,7]) which points out the importance of grain boundaries in the development of gas porosity. For gaining a deeper insight into helium behavior the implantation of Be with He ions is frequently used [5], and both helium remission [9] and helium thermal desorption [10,11] are studied which is of a great concern for fusion applications.

The aim of this work was to study the development of helium porosity development in Be with a well characterized microstructure as a function of irradiation and/or annealing temperature. Using this information we hoped to understand the peculiarities of He reemisson [9], some contradictions in thermal desorption results reported in [10,11] and to compare the development of He bubbles with that of D_2 cavities due to D ion implantation [12].

2. Experimental

TIP-30 beryllium was used, manufactured by A.A. Bochvar Institute (VNIINM, Moscow) by hot isostatic

* Corresponding author. Tel.: +49 2461 61 3160; fax: +49 2461 61 2410.

0022-3115/98/$19.00
PII: S0022-3115(98)00250-5

pressing, containing about 2.2 wt% of BeO, having an average grain size of 20 μm and accumulating about 1% of porosity in grain boundaries, triple junctions and in connection with second phase inclusions [13]. The implantation with 5 keV (projected range $\overline{R}_p = 65$ nm, straggling $\sigma = 20$ nm) and 15 keV ($\overline{R}_p = 150$ nm, $\sigma = 30$ nm) He ions at T_{irr} up to 700 K was performed up to fluences of $\Phi = 4.5 \times 10^{21}$ He m^{-2} in an UHV setup described in [14]. Some implanted specimens were annealed at T_{ann} up to 1100 K for 10 min in an oil free vacuum of $(3 \pm 1) \times 10^{-4}$ Pa. Next to implantation (and annealing) the specimens were back-thinned electrolytically from the side opposite to the irradiated one and investigated in TEM EM-400T and EM-430 operated at 120 and 300 kV, respectively.

3. Results and discussion

3.1. Helium bubbles at $T_{irr} \leqslant 500$ K

At $T_{irr} = 300$ and 500 K, small helium bubbles with a mean radius, $\overline{r}_b \cong 0.8$ nm and a mean volume density, $\overline{c}_b \cong 4.5 \times 10^{24}$ m^{-3} are observed in Be implanted with 5 keV He ions to a dose of $\Phi = 3 \times 10^{20}$ He m^{-2} (corresponds to a He concentration of 4.5 at.% in the peak region). In this case, the resulting gas swelling, S, within the near-surface layer of 50 nm thickness is less than 1%. The formation conditions and parameters of these bubbles suggest that they are overpressurized [4,15], i.e. the mean gas pressure, p_g therein is significantly higher than the equilibrium pressure $\overline{p}_g^{\sigma} = 2\gamma/\overline{r}_b$, where $\gamma = 3.13$ J m^{-2} is the specific surface energy of Be [12].

Similar to other metals, the abrupt reemission of implanted He from Be observed in [9] at $\Phi_c = 2 \times 10^{21}$ He m^{-2} seems to be a result of helium bubble interaction. In this case, apart from blistering, the formation of microchannels (similar to those appearing during D ion implantation [12]) is highly probable. Indeed, at $\Phi = 3 \times 10^{21}$ He m^{-2} we clearly register strings of interconnected He bubbles (microchannels) by TEM. At higher fluences the developing open channels, which short-circuit the near-surface layers of Be, are responsible for the higher remission rates observed [9]. The formation of open channels is also evidenced by the results on oxygen sorption within the near-surface layers of Be implanted with 6 keV He ions up to $\Phi \geqslant (5 \pm 1) \times 10^{21}$ He m^{-2} [16].

For $T_{irr} = 300$ K the parameters of He bubbles are reminiscent of those of D_2 cavities [12]. Also thermal desorption spectra of He and D_2 introduced into Be by means of ion implantation were shown to have much in common [17], but the underlying processes of bubble coarsening differ noticeably (see Sections 3.3 and 3.4).

3.2. Helium bubbles at $T_{irr} = 700$ K

The helium porosity formed during He ion implantation at 700 K differs significantly from that at $T_{irr} = 500$ K. A typical microstructure of Be implanted at 700 K with 15 keV He ions to $\Phi = 2 \times 10^{21}$ He m^{-2} is presented in Fig. 1a. Along with grains having blister caps, grains completely devoid of their caps are frequently found (bright area in the lower right hand part). The latter regions are convenient for observing details of the bubble morphology because within these particular areas the foil thickness is reduced by $\approx \overline{R}_p \cong 150$ nm (Fig. 1(b)). It is found that the mean sizes of bubbles developed at 700 K in the bulk and at the grain boundaries are identical, and they are facetted. As compared to $T_{irr} \leqslant 500$ K, the bubbles developing at 700 K are significantly larger: $r_b \geqslant 10$ nm in the peak region of the implantation profile and $\overline{r}_b \cong 4$–5 nm at its tails.

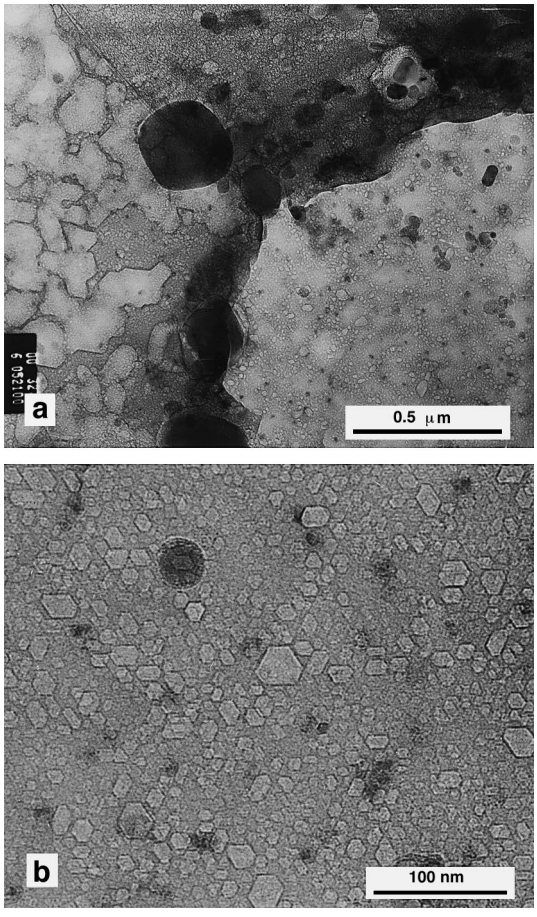

Fig. 1. Microstructure of Be implanted with 15 keV He ions to $\Phi = 2 \times 10^{21}$ He m^{-2} at 700 K: (a) general view; on the right the grain area is devoid of a surface layer due to blistering; (b) helium bubbles formed under blister cap at a depth $\geqslant 150$ nm.

In spite of their much smaller volume density, these large sized bubbles give rise to high values of gas swelling, S, which even at a depth $> \overline{R_p}$ is in excess of 5%.

It is worth noting that our observation of high gas swelling at $T_{irr} = 700$ K falls within the temperature range where swelling in Be irradiated by fast neutrons (to relatively low fluences) sets in [5,13]. This coincidence and the fact that S keeps increasing with T_{irr} (instead of showing the void swelling maximum at $T_{irr} \approx 0.45T_m$) strongly suggest that the volume increase in neutron irradiated Be is in fact gas driven.

In between blisters, at a depth of $\overline{R_p}$, mainly coarse and oblate gas cavities of irregular shape develop and make the main contribution to the local swelling (see left-hand side in Fig. 1(a)). Their arrangements are orientation dependent and they are reminiscent of the oblate labyrinth structures in Be implanted with D ions at the same T_{irr} [12]. On the other hand, the lateral dimensions of coarse He cavities (Fig. 1(a)) and the mean sizes of facetted He bubbles (Fig. 1(b)) are, respectively, much lower than those of corresponding D_2 filled cavities [12].

The abrupt reemission increase of implanted He at $T_{irr} = 675$ K [9] is, obviously, a result of a high temperature blistering which takes place as a consequence of the coalescence of He bubbles and cavities occurring at a depth $\cong \overline{R_p}$. Gas filled microchannels do not form at such temperatures. The fact that the increase of T_{irr} from 300 to 675 K shifts the onset of an abrupt gas reemission noticeably towards lower fluences [9], is a consequence of the much higher gas swelling in the near-surface layers of Be at $T_{irr} = 675$ K compared to that at $T_{irr} = 300$ K. In the case of D ion implantation such an effect of a Φ_c shift is practically absent [12] because the kinetics of the deuterium swelling build-up when increasing T_{irr} is smoothed out due to: (a) some limited deuterium remission starting at T_{irr} as low as $\leqslant 500$ K [18] and (b) the considerably lower bulk modulus, B_T^{D2}, of deuterium (that is D_2 softness) compared to B_T^{He} of helium for relatively high atom densities within gas cavities; here $B_T = -V(\partial p/\partial V)_T$, where p is the inner gas pressure and V is the cavity volume.

3.3. Helium swelling at post-implantation annealing

According to [19–22] a clear correlation exists between the temperature of post-implantation annealing where helium-induced swelling of a metal increases rapidly and the dissociation temperature of HeV complexes, T_{HeV}^D. Bearing this in mind and taking into account the data in Refs. [5,7] on gas swelling kinetics during annealing after low temperature neutron irradiation, one can estimate T_{HeV}^D for Be to be around 900 K. This value corresponds to a dissociation energy of HeV complexes, $E_{HeV}^D(\text{Be}) \approx 2.2$ eV. On the homologous temperature scale the above temperature corresponds to $0.57\ T_m(\text{Be})$, which is close to the known T_{HeV}^D values for Ni ($0.53\ T_m$) and Cu ($0.58\ T_m$) [21].

In Fig. 2 are shown helium bubbles in Be implanted with 5 keV He ions to $\Phi = 3 \times 10^{20}$ He m^{-2} at 500 K and subsequently annealed at $T_{ann} = 950$, 1000 and 1100 K, respectively, for 10 min. Gas losses during annealing are negligible [17]. In general, annealing a temperature 950 K $> T_{HeV}^D$ should lead to noticeable bubble coarsening and swelling increase, because then He atoms are no longer bound to vacancies, and the outer surface plays mainly a role of an efficient vacancy source. Indeed,

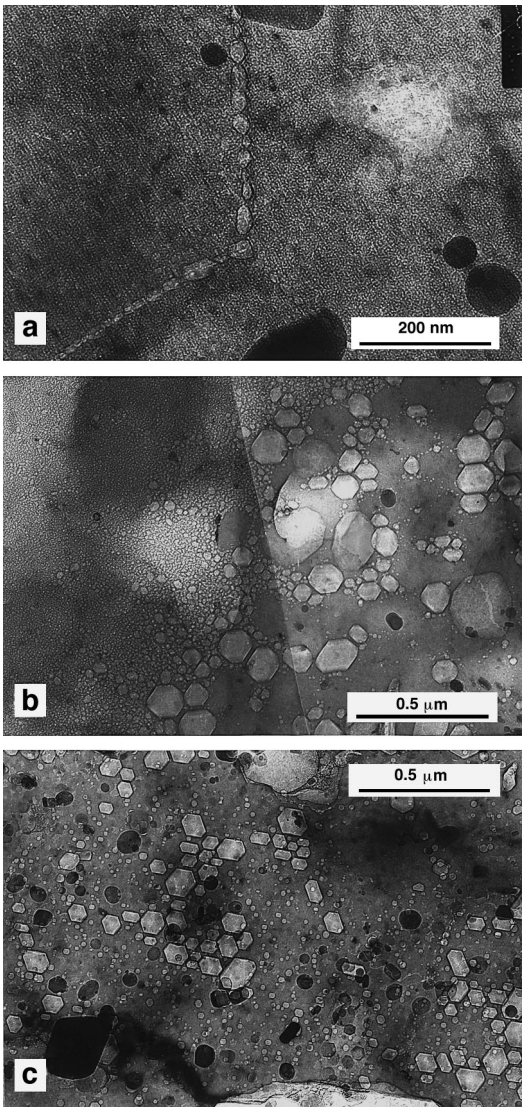

Fig. 2. Helium bubbles in Be implanted with 5 keV He ions to $\Phi = 3 \times 10^{20}$ He m^{-2} at 500 K and annealed for 10 min at: (a) 950 K, (b) 1000 K and (c) 1100 K (cf. magnifications in (a) and (b), (c)).

annealing at 950 K caused only a small increase of the mean radius of bubbles, while larger and facetted bubbles with $\bar{r}_b \cong 10$–12 nm were formed along grain boundaries (GBs) (Fig. 2(a)).

Due to annealing at 1000 K the mean bubble radius increases remarkably not only at GBs ($\bar{r}_b \approx 30$ nm), but also near them ($\bar{r}_b \leqslant 30$ nm), and most of the large bubbles become facetted. Simultaneously, very small bubbles with $\bar{r}_b \leqslant 3.0$ nm and high $\bar{c}_b$ values (of 10^{23} m^{-3}) are retained in the same specimens, and are most commonly observed in the central parts of large grains.

In specimens annealed at 1100 K He bubbles are characterized by $\bar{r}_b \cong 9$ nm, while the fraction of small bubbles with $r_b < 3$ nm is only of one tenth of the total bubble number. The size distribution of gas cavities is more or less identical throughout the implanted layer, and there are no very large bubbles at GBs (Fig. 2(c)). Here the dislocation density within the ion range is significantly lower than in specimens annealed at 950 and 1000 K.

According to Refs. [20,21], post-implantation annealing of fcc-Ni and Cu loaded homogeneously with He (by α-particle implantation) at $T_{ann} > T^{D}_{HeV}$ results in the appearance of two populations of He filled cavities, namely: tiny overpressurized (*primary*) bubbles in the bulk of grains and large, nearly equilibrium (*secondary*) gas cavities at and near GBs. We suppose that our data on the microstructure of Be after post-implantation annealing at 950 and 1000 K are indicative of a similar formation of two different kinds of gas cavities. In this case, in contrast to Refs. [20,21], we deal with only a thin He implanted layer of metal near the outer surface. Since a vacancy deficit is a necessary requirement for the existence of overpressurized bubbles, this surface must be unable to supply thermal vacancies [21], and we assume that oxide film covering the surface is the reason for this.

The role of an oxide film as a vacancy barrier was demonstrated in Ref. [23] for cph-Zn covered by ZnO. But, whereas in the cited work the vacancy barrier provided a vacancy supersaturation in the metal bulk, the layer of BeO (of the same structure type as ZnO) on the surface of some beryllium grains is a barrier causing the retention of the vacancy deficit within the implanted metal layer. The above difference in the roles of oxide films on the surface of Zn and Be, respectively, is related to the difference in their oxidation conditions and growth kinetics [23,12]. An area of the BeO film on the surface of He implanted and annealed Be is presented in Fig. 3. In contrast to fine-crystalline oxides registered on the surface of electropolished Be this film has a greater thickness, consists of larger cph-BeO microcrystals and is porous (just as that after D ion implantation [12]). The size of BeO microcrystals depends on the annealing temperature and is about 16 nm in the case shown in Fig. 3.

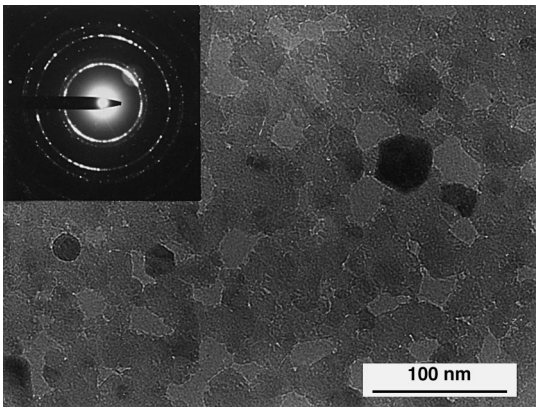

Fig. 3. Fine-crystalline film of cph-BeO oxide of about 16 nm thickness on the surface of Be implanted with 5 keV He ions to $\Phi = 3 \times 10^{20}$ He m^{-2} at 500 K and annealed at 1100 K for 10 min; underfocused image in phase contrast. The insert is a selected area diffraction pattern from a BeO film area of 0.5 μm in diameter.

In contrast to the oxide-covered outer surface, the grain boundaries act as efficient vacancy sources which is evidenced by high gradients in the bubble size in directions from the interior to the periphery of large grains in the specimens annealed at 1000 K (Fig. 2(b)). Gradients of that kind are caused by a rapid coarsening of primary gas bubbles near vacancy sources [20,21,24]. The presence of anomalously large cavities and long tails at the bubble size distributions of secondary bubbles compared to those in Ni [20] and Cu [21] are attributed to the high intrinsic porosity of this grade of beryllium (see Section 2) and a possible dependence of the performance of the BeO surface film as a vacancy barrier on the orientation of a matrix grain relative to the outer surface. Another reason for the appearance of anomalously large cavities could be the reaction of Be with residual water vapor: $Be + H_2O \rightarrow BeO + H_2 \uparrow$. The liberated hydrogen can partly enter the near-surface layers and can facilitate cavity coarsening [12,25] (see also Section 3.4).

According to [21], the overpressure in primary He bubbles in Ni and Cu is retained under conditions of vacancy deficit in the matrix at temperatures $\leqslant 0.72T_m$. In this temperature range edge dislocations are incapable of emitting vacancies into the volume due to "poisoning" by He atoms. At $T_{ann} \geqslant 0.72T_m$ dislocations recover this ability which makes the pressure in primary bubbles to relax giving rise to a change of the coarsening mechanism of resultant bubbles. Following [26], this leads to the formation in Ni of a single ensemble of bubbles throughout the volume. This process is accompanied by a decrease of the dislocation density. It is these signs which distinguish the population of He bubbles (Fig. 2(c)) and the corresponding dislocation

structure which form in He implanted Be at $T_{ann} \geqslant 1100$ K (0.70 T_m) from those formed at $\leqslant 1000$ K (Fig. 2(a) and (b)). Probably, the processes taking place during annealing of helium loaded Be and Ni at $T_{ann} \geqslant 0.72\ T_m$ bear not only an outer resemblance, but are of identical nature. In this case the homologous temperature of the recovery of dislocations poisoned by helium in Be, $T_R(\text{Be}) \approx 0.7 T_m(\text{Be})$ is close to the corresponding values for Ni and Cu [21].

3.4. Comparison of He and D_2 bubble coarsening

The parameters of bubbles, formed in Be at 300 K due to irradiation by He and D ions, respectively, are very similar. This is no accident since the deuterium solubility in Be at 300 K is also very small [27].

With increasing irradiation temperature the coarsening of D_2 bubbles is registered at $T_{irr} \leqslant 500$ K $< T^D_{DV} \approx 670$ K [12,28], and that of He bubbles occurs at $T_{irr} \leqslant 700$ K which is also below T^D_{HeV}, i.e. in both cases the coarsening must be due to athermal (displacement) resolution. The observed temperature difference in the onset of coarsening seems to be a consequence of the higher binding energy in HeV complexes ($E^D_{HeV} \approx 2.2$ eV) compared to that in DV ($E^D_{DV} \approx 1.7$–1.8 eV [12,28]). It means that the binding energy "gas atom-vacancy" is a parameter which determines the onset of gas porosity development not only during post-implantation annealing [20–22], but also under irradiation.

The slower development of He bubbles than that of D_2 bubbles holds also at higher temperatures as seen from a comparison of both results of annealing experiments and parameters of bubbles formed during ion implantation (cf. He bubble parameters in the present work with those of D_2 bubbles in Refs. [12,25]). The main reasons for these differences are the much higher mobility of D atoms [28] compared to that of He atoms [29], the incomparably higher solubility of deuterium in Be at elevated temperatures [27] and, possibly, a chemical activity of deuterium on the cavity surfaces which facilitates the coarsening process [12].

In the course of annealing of Be implanted with D and He ions at $T_{ann} \geqslant T^D_{DV}$ and T^D_{HeV}, respectively, D_2 bubbles coarsen throughout the whole implanted volume (Fig. 4(b) in Ref. [12]), while He bubbles coarsen mainly at and near GBs (Fig. 2(a) and (b)). In the latter case the coarsening of primary bubbles takes place due to gradual relaxation of their *overpressure* near adjacent vacancy sources, in particular, GBs (see Section 3.3) [21]. We have no reasons to consider D_2 cavities as overpressurized, not only when reaching $T_{ann} = T^D_{DV}$, but also just after implantation [12] which explains the absence of preferential D_2 bubble coarsening near GBs.

4. Summary

The implantation of beryllium with 3 and 15 keV He ions in the temperature range from 300 to 700 K up to fluences $\Phi < 3 \times 10^{20}$ He m^{-2} leads to the formation of gas filled bubbles and cavities, while at $\Phi \geqslant 2 \times 10^{21}$ He m^{-2} blistering occurs. At $T_{irr} \leqslant 500$ K tiny and presumably overpressurized He bubbles ($\bar{r}_b \leqslant 1$ nm) of a high volume density arise which show a tendency to form interconnected microchannels at doses of $>2 \times 10^{21}$ He m^{-2}. At $T_{irr} = 700$ K facetted bubbles with radii in the range from 1 to 10 nm are developed together with more capacious oblate gas cavities at a depth of $\bar{R}_p$.

The corresponding swelling values indicate that the enhanced volume increase observed in neutron-irradiated Be for $T_{irr} \geqslant 700$ K is the gas-induced swelling due to helium and, most probably, tritium [30] produced by nuclear reactions.

The dissociation temperature of HeV complexes, T^D_{HeV}, in Be is definitely lower than 950 K, but higher than that of DV complexes (≈670 K). During post-implantation annealing the behavior of helium porosity in cph-Be has common features with that in fcc-Ni and Cu homogeneously loaded with helium [19–21]. The oxide layer of cph-BeO which forms on the surface of Be under He ion implantation and annealing is expected to be a barrier for thermal vacancies, at least up to 1000 K, and it is believed that overpressurized bubbles can temporary survive in Be at $T_{ann} > T^D_{HeV} \approx 900$ K.

Under identical experimental conditions the coarsening of He bubbles in Be proceeds much slower than that of D_2 bubbles. This is related to differences in the solubility of He and D_2 in Be and in the mobility of He and D atoms in this metal. Other factors of influence are differences in the dissociation energies of HeV and DV complexes and the compressibility of helium and deuterium at high gas densities, and deuterium chemical activity, respectively.

Swelling of Be under fast neutron irradiation is in fact gas induced swelling mainly due to helium available through nuclear transmutations.

Acknowledgements

The authors thank Dr.V. Kh. Alimov (IPhCh) for the implantations of beryllium specimens with He ions.

Obituary: In April 1998, Dr. V.N. Chernikov died of an insidious disease. His unexpected death leaves a gap in the fusion materials community. Many of us have lost in him not only a colleague but also a good friend. We mourn for Vladimir.

References

[1] ITER Conceptual Design, Interim Report, IAEA/ITER/DS/7, IAEA, Vienna, 1990.

[2] K.L. Wilson, R.A. Causey, W.L. Hsu, B.E. Mills, M.F. Smith, J.B. Whitley, J. Vac. Technol. A 3 (8) (1990) 1750.

[3] M.C. Billone, M. Dalle Donne, R.G. Macaulay-Newcombe, Status of Beryllium Development for Fusion Applications, in: Third International Symposium on Fus. Nucl. Technol., UCLA, 27 June–1 July 1994.

[4] A.M. Khomutov, D.A. Davydov, V.A. Gorokhov, I.B. Kuprijanov, V.S. Mikhailov, Ya.D. Pakhomov, J. Nucl. Mater. 233–237 (1996) 111.

[5] D.S. Gelles, G.A. Sernyaev, M. Dalle Donne, H. Kawamura, J. Nucl. Mater. 212–215 (1994) 29.

[6] C.E. Ells, E.C.W. Perryman, J. Nucl. Mater. 1 (1959) 73.

[7] J.B. Rich, G.B. Redding, R.S. Barnes, J. Nucl. Mater. 1 (1959) 96.

[8] G.A. Sernyaev, Voprosy Atomnoj Nauki i Techn. 2 (56) (1991) 16.

[9] A.E. Pontau, W. Bauer, R.W. Conn, J. Nucl. Mater. 93/94 (1980) 564.

[10] J.P. Biersack, D. Fink, R.A. Henkelmann, K. Möller, J. Nucl. Mater. 85&86 (1979) 1165.

[11] H. Eleveld, A. van Veen, F. Labohm, M.W. de Moor, J. Nucl. Mater. 212–215 (1994) 972.

[12] V.N. Chernikov, V.Kh. Alimov, A.V. Markin, A.P. Zakharov, J. Nucl. Mater. 228 (1996) 47; a short version of the same paper see in: V.N. Chernikov, V.Kh. Alimov, A.V. Markin, A.E. Gorodetsky, S.L. Kanashenko, A.P. Zakharov, I.V. Kupriyanov, J. Nucl. Mater. 233–237 (1996) 860.

[13] I.B. Kupriyanov, V.A. Gorokhov, A.M. Khomutov, Manufacturing and some properties of powder beryllium with high radiation stability, in: Fusion Technology 1994, Proceedings of Eighteenth Symposium on Fus. Technol. Part I, Karlsruhe, 22–26 August 1994, Elsevier, Amsterdam, 1995, pp. 423–426.

[14] V.Kh. Alimov, V.N. Chernikov, A.P. Zakharov, J. Nucl. Mater. 241–243 (1997) 1047.

[15] A.G. Zaluzhny, Yu.N. Sokursky, V.N. Tebus, Helium in Reactor Materials (in Russian), Energoatomizdat, Moscow, 1988, p. 89.

[16] V.Kh. Alimov, R.Kh. Zalavutdinov, A.E. Gorodetsky, A.P. Zakharov, J. Nucl. Mater. 220–222 (1995) 947.

[17] A.V. Markin, V.N. Chernikov, S.Yu. Rybakov, A.P. Zakharov, in: Proceedings of Second IEA International Workshop on Beryllium Technology for Fusion, 6–8 September 1995, Jackson Lake Lodge, Wyo., CONF-9509218, Lockheed Martin Idaho Technologies, Idaho Falls, 1995, pp. 332–347.

[18] Möller, B.M.U. Scherzer, J. Bohdansky, IPP-JET Report No. 26, 1986.

[19] V.N. Chernikov, A.P. Zakharov, P.R. Kazansky, J. Nucl. Mater. 155–157 (1988) 1142.

[20] V.N. Chernikov, H. Trinkaus, P. Jung, H. Ullmaier, J. Nucl. Mater. 170 (1990) 31.

[21] V.N. Chernikov, J. Nucl. Mater. 195 (1992) 29.

[22] V.N. Chernikov, Ju.V. Lakhotkin, H. Ullmaier, H. Trinkaus, P. Jung, H.J. Bierfeld, J. Nucl. Mater. 212–215 (1994) 375.

[23] V.N. Rozhansky, A.A. Predvoditelev, V.L. Indenbom, Soviet Phys. – Solid State 9 (1967) 593 (in Russian).

[24] H. Trinkaus, Scripta Metall. 23 (1989) 1773.

[25] N. Yoshida, S. Mizusawa, R. Sakamoto, T. Muroga, J. Nucl. Mater. 233–237 (1996) 874.

[26] V.N. Chernikov, H. Trinkaus, H. Ullmaier, J. Nucl. Mater. 250 (1997) 103.

[27] V.I. Shapovalov, Yu.M. Dukelskii, Russ. Metallurgy 5 (1988) 210.

[28] W.R. Wampler, J. Nucl. Mater. 196–198 (1992) 981.

[29] P. Jung, J. Nucl. Mater. 202 (1993) 210.

[30] D.V. Andreev, V.N. Bespalov, A.Ju. Birjukov, B.A. Gurovich, P.A. Platonov, J. Nucl. Mater. 233–237 (1996) 880.